

## Dynamic oscillations in the supercritical carbon dioxide natural circulation loop

Draskic, Marko; Nelissen, Isabelle M.E.; Pecnik, Rene

**DOI**

[10.1016/j.ijheatmasstransfer.2025.127206](https://doi.org/10.1016/j.ijheatmasstransfer.2025.127206)

**Publication date**

2025

**Document Version**

Final published version

**Published in**

International Journal of Heat and Mass Transfer

**Citation (APA)**

Draskic, M., Nelissen, I. M. E., & Pecnik, R. (2025). Dynamic oscillations in the supercritical carbon dioxide natural circulation loop. *International Journal of Heat and Mass Transfer*, 250, Article 127206. <https://doi.org/10.1016/j.ijheatmasstransfer.2025.127206>

**Important note**

To cite this publication, please use the final published version (if applicable). Please check the document version above.

**Copyright**

Other than for strictly personal use, it is not permitted to download, forward or distribute the text or part of it, without the consent of the author(s) and/or copyright holder(s), unless the work is under an open content license such as Creative Commons.

**Takedown policy**

Please contact us and provide details if you believe this document breaches copyrights. We will remove access to the work immediately and investigate your claim.



# Dynamic oscillations in the supercritical carbon dioxide natural circulation loop

Marko Draskic<sup>ID\*</sup>, Isabelle M.E. Nelissen<sup>ID</sup>, Rene Pecnik

Department of Process & Energy, ME, TU Delft, Leeghwaterstraat 39, Delft, 2628 CB, The Netherlands

## ARTICLE INFO

### Keywords:

Experiments  
Natural circulation loop  
Instability  
Supercritical

## ABSTRACT

Supercritical natural circulation loops (NCLs) promise passive cooling for critical systems like nuclear reactors and solar collectors, eliminating the need for mechanical pumps. However, instabilities similar to those seen in two-phase systems can emerge in supercritical NCLs, leading to undesirable oscillatory behaviour, marked by system-wide fluctuations in density, temperature, pressure, and flow rate. This study investigates the stability of NCLs at supercritical pressures ( $73.7 \leq p \leq 110.0$  bar) using CO<sub>2</sub> in an experimental setup with vertical cooling and vertically adjustable heaters to control convective flow rates and to oppose flow reversal. Oscillations were found to originate in the heater of the NCL, and demonstrated a high sensitivity to the thermodynamic state and proximity to the pseudo-critical line of the system. Increased mass flow rates and added resistance upstream of the heater suppressed the oscillations, while increased pressures and reduced heating rates dampened them. A static model which takes into account the non-ideality of the heat exchangers is introduced to assess the presence of multiple steady states. The system is concluded to be statically stable, and the oscillations are considered to be dynamically induced. In particular, the modulation of the NCL velocity by the traversal of the current oscillations in density is assumed to periodically re-ignite non-ideality in the heater. These findings intend to refine our understanding of the stability boundaries in NCLs, to ensure a safer operation of prospective passive cooling and circulation systems employing fluids at supercritical pressure.

## 1. Introduction

When a closed flow loop is heated at one of its vertical legs and cooled at the other, a natural circulation is induced. Such Natural Circulation Loops (NCLs) are passive circulators, as they do not rely on mechanical propulsion for fluid flow. This makes them particularly attractive for off-grid cooling applications in critical systems, such as nuclear reactors and solar thermal systems, when nearby heat sinks are available for effective heat dissipation. When the induced mass flow rates of the reliable natural circulators are sufficient, they can potentially replace their existing forced convective counterparts.

Two-phase circulation loops, in particular, offer substantial potential for energy transport due to the significant volumetric expansion of their phase transitions. However, two-phase systems are often prone to dynamic instabilities, associated with the phase-change phenomena within the loop [1,2]. These instabilities can lead to substantial flow oscillations and dry-out, limiting the reliability of potential passive circulators with large heating loads.

In response to these challenges, NCLs with fluids at supercritical pressures have emerged as a promising alternative. At a supercritical pressure, a fluid no longer discretely transitions from its liquid to its gas

state. Instead, the heating and cooling of a supercritical fluid is characterized by large variations in thermophysical properties, whilst the fluid effectively remains in a single continuous phase. The variations in thermodynamic properties are particularly large in the vicinity of the *pseudo-critical* curve (p-c curve), an extension of the vapour-liquid coexistence curve in the supercritical region. The location of the p-c curve, as defined by Banuti [3], is indicated in Fig. 1. Furthermore, Figs. 1(c) and 1(d) respectively show the variation in density  $\rho$  and viscosity  $\mu$  near the p-c curve at the isobars defined in Fig. 1(a). As suggested by the inverse of Fig. 1(c), the dilation of the CO<sub>2</sub> in the NCL heat exchangers can be substantial, especially in the near-pseudo-critical region. As such, much like two-phase systems, NCLs with working fluids at supercritical pressures can yield passive flow rates of a sufficient magnitude for the removal of nuclear and concentrated solar heat. However, whereas complex phase-change behaviour is in principle avoided at a supercritical pressure, supercritical pressure NCLs are still prone to several analogous instabilities.

For natural circulation loops, the classification of flow instabilities in two-phase systems is generally extended into the supercritical region [4,5]. Therewith, a distinction is made between statically and

\* Corresponding author.

E-mail addresses: [M.Draskic@tudelft.nl](mailto:M.Draskic@tudelft.nl) (M. Draskic), [r.pecnik@tudelft.nl](mailto:r.pecnik@tudelft.nl) (R. Pecnik).

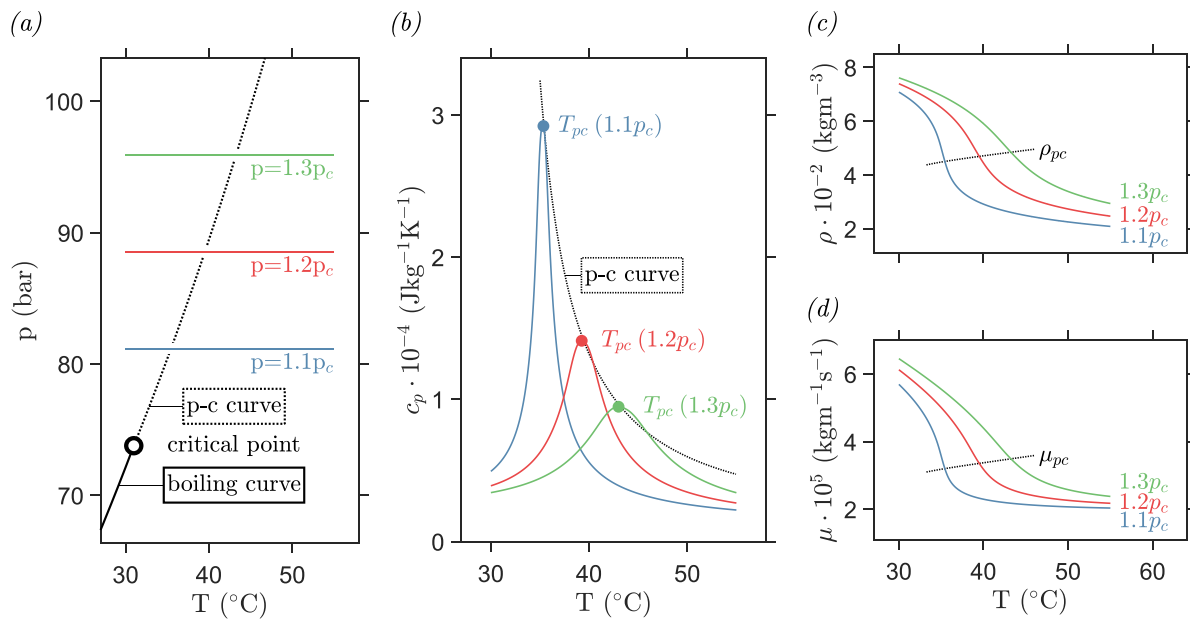


Fig. 1. Thermodynamic properties of carbon dioxide at supercritical pressures, for which the critical temperature and pressure are at  $T_c = 31.0$  °C and  $p_c = 73.8$  bar, respectively. (b): shows the isobaric heat capacity  $c_p$  along the isobars that are indicated in the phase diagram in (a). The pseudo-critical (p-c) curve is defined at the local maxima of  $c_p$  along an isobar [3]. Distributions of density  $\rho$  and viscosity  $\mu$  for the current isobars are shown in (c), respectively.

dynamically unstable flow systems [1,2]. When an NCL is statically unstable, multiple steady state solutions exist that satisfy the conservation equations. Then, perturbations within the NCL can lead to single-event or repeating excursions that shift the system between steady states. An instability is considered dynamic when the system requires a feedback mechanism to develop and sustain unsteady behaviour [1]. As such feedback effects are not captured in static models, a model of the steady state by itself is not sufficient to predict a system's dynamic stability limits. So far, the dynamic stability of supercritical CO<sub>2</sub> NCLs has most commonly been studied in the context of Density Wave Oscillations (DWOs) and Pressure Density Oscillations (PDOs), whereas static instabilities have mainly been of the above-discussed Ledinegg type [4–6].

The dynamic stability of natural circulation loops (NCLs) at supercritical pressures has been extensively modelled. Although three-dimensional analyzes have been undertaken [7,8], most numerical studies model NCLs using non-linear one-dimensional approaches. Most commonly, a boundary heating rate has been presented as the stability threshold, beyond which instabilities occur [7,9–13]. This threshold has been found to be sensitive to several operating parameters, such as the heater inlet temperature [9,11,12], the system pressure, its mass flow rate [8], and the loop diameter [14]. Using linearized one-dimensional models, the thermodynamic dependence of the stability limit has been elaborated on Debrah et al. [13], Ambrosini and Sharabi [15]. Furthermore, the dynamic stability of an NCL has been found to be strongly affected by the configuration of the heat exchangers. When all heat is exchanged along the horizontal legs of the system, the NCL has no preferential flow direction. Then, the NCL is prone to flow reversal. In a system with heat exchange along at least one of its vertical legs, the vertical line symmetry is broken. As a result, the risk of flow reversal instabilities is greatly reduced [7,8,16–18], substantially increasing the stable heating threshold.

Moreover, to assess whether static instabilities can prevail in a supercritical pressure NCL, the system can be investigated for the presence of multiple steady states. The driving pressure of a loop (resulting from a density difference over its vertical legs) balances with its viscous friction ( $\Delta p_v$ ) throughout the system to circulate CO<sub>2</sub>. At any possible steady state, the two quantities are equal. If multiple steady states exist – at multiple mass flow rates – the system may transition to different

steady states upon a perturbation, or alternate between various steady states, resulting in limit cycle oscillations [2,4,19]. When an ideal sub-critical friction model is used in the static model, ignoring the effects of thermodynamic property variations, the CO<sub>2</sub> NCL is predicted to be statically stable [6,20–22].

The stability of NCLs at supercritical pressures has also been explored experimentally. The earliest reports of unstable behaviour in the supercritical pressure NCL considered the symmetric horizontal-heater-horizontal-cooler (HHHC) configuration [23,24], for which the mass flow rate is maximized, but flow reversal are more prevalent [21]. Most investigations of non-HHHC loops that followed reported stable behaviour within the considered parameter ranges when the NCL was not externally forced [18,25,26]. However, Huang et al. [22], Liu et al. [27] later reported oscillations in this non-HHHC setting, in which heat is transferred along the vertical legs of the system. In Huang et al. [22], a parallel-channel vertical heater within an NCL was investigated for instabilities. The authors reported irregular PDO's in the vicinity of the pseudo-critical curve that were strongly influenced by the presence and position of a large pressurizer. In the work of Liu et al. [27], a departure from stability was observed in a single-channel supercritical CO<sub>2</sub> NCL. Unlike system-wide density-wave oscillations, the temperature oscillations were limited to the NCL heater outlet. The oscillations were most predominantly found in the vicinity of the pseudo-critical curve. Similarly to Huang et al. [22], an increase in pressure was found to stabilize the system, likely due to a reduction in thermal property variations near the pseudo-critical line. Additionally, the presence of a local resistance was reported to enhance or lessen the stability of the NCL, depending on the placement of the local loss [27].

The current study experimentally investigates the stability of a natural circulation loop at supercritical pressure. In particular, an NCL with all heat exchange along its vertical legs is considered. Given its enhanced stability and its reduced sensitivity to flow reversal, this configuration in particular is promising for stable passive circulators and coolers with large throughputs for high-energy application. Nevertheless, even for this most stable heating configuration, an eventual limit to the stability of an NCL has been predicted in simulations. However, these predictions are largely based on one-dimensional models that necessarily rely on strong simplifications—particularly in the treatment of wall friction and heat transfer under highly non-ideal conditions.

**Table 1**  
Dimensions of current natural circulation loop, shown in Fig. 2.

Parameter & description		Value	Unit
H	loop height	4.0	m
L	loop length	10.0	m
D	inner diameter	21.1	mm
D <sub>o</sub>	outer diameter	25.4	mm
Δz	driving height	≤2.5	m

As such, experimental validation is essential to support these models and assess the accuracy of their predicted stability limits. To date, little experimental evidence of unsteady behaviour has been presented. While substantial local oscillations in heat exchangers have been reported [22,27], global, system-wide oscillations in a single-channel NCL that resemble the predictions from numerical modelling have not yet been demonstrated in experiment. Therefore, the current experiments aim to identify and cross the stability limits of a supercritical NCL in the present configuration, to ultimately support the development of mitigation strategies and help prevent potentially catastrophic thermal fatigue in full-scale systems.

The current experimental setup facilitates substantial non-ideal expansions of carbon dioxide at supercritical pressures, with which the previously predicted limits of stability are approached. Contrary to other existing systems, the current facility employs heaters that can be moved vertically. By decreasing the vertical distance between the heating and cooling elements the mass flow rate of the NCL can be controlled and greatly reduced, even without a local resistance in the system. As such, the strong pseudo phase-change behaviour within full-scale high-energy natural circulation loops can be emulated with heating rates attainable in a laboratory setting, without local restrictors that may delay the onset of instability. Consequently, we have successfully incited system-wide sustained oscillations in temperature, pressure and mass flow rate in a natural circulation loop with CO<sub>2</sub> at supercritical pressures. The current experiments consider the system's sensitivity to operating conditions and inputs, to explore the stability of large throughput passive circulators previously not touched upon in experiment.

A description of the experimental facility is given in 2.1 of Section 2. Furthermore, a simplified static model of the heater with which the stability mechanism is explored is proposed in 2.2 of Section 2. In Section 3, the perceived saturated oscillations are first described. Thereafter, the system's sensitivity to its operating conditions and inputs is assessed, and oscillation mitigation measures are proposed. Thereafter, possible instability mechanisms are discussed in Section 4. Finally, a summary of the most important conclusions is presented in Section 5.

## 2. Methodology

In this work, the oscillatory behaviour of the supercritical natural circulation loop is studied experimentally. Additionally, the heat exchangers are analyzed with a one-dimensional static model to support the discussion of the perceived instability. Hereafter, the current experimental facility and the static model are introduced in respective sub-sections.

### 2.1. Experimental methodology

#### 2.1.1. Experimental facility

The current experimental facility is based on the system introduced in Draskic et al. [28]. A schematic of the experimental facility is shown in Fig. 2. The dimensions of the facility are given in Table 1. The main natural circulation loop is indicated with a thick black closed line. One vertical leg of the NCL is cooled with a tube-in-tube counter-current heat exchanger (which is baffled on the coolant side), shown in blue in the top left of the figure. The inlet temperature of the cooler

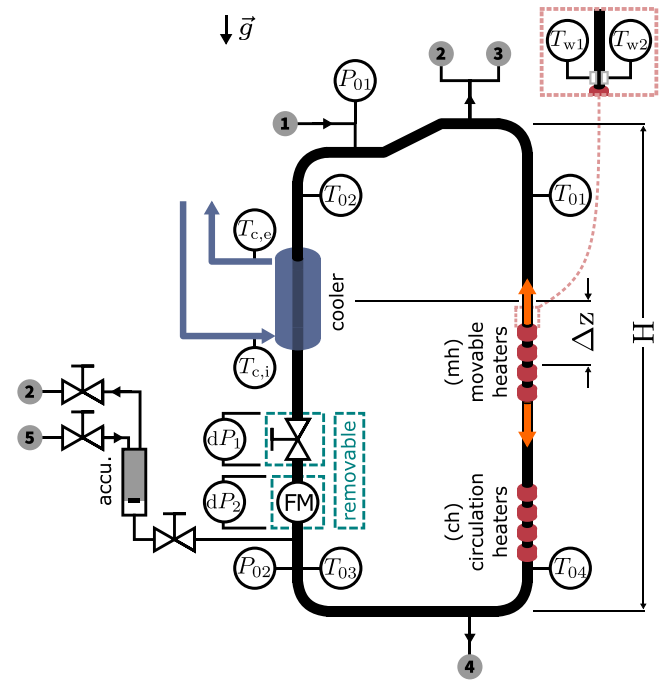


**Fig. 2.** Schematic of the current natural circulation loop (NCL). The main flow loop is indicated with a thick black line. The system is connected to ① a CO<sub>2</sub> bottle with a dip tube, ② a purge that is connected to the laboratory's gas vent system, ③ a vacuum pump, ④ a drain, and ⑤ a nitrogen bottle. The electric heating elements and the annular cooler are indicated in red and blue, respectively. The top-most electric heaters (labelled *mh*) can be translated vertically. All removable elements are outlined with a green dotted line. Temperature-, absolute pressure- and mass flow rate transmitters are indicated with  $T_x$ ,  $P_x$  and FM, respectively. (For interpretation of the references to colour in this figure legend, the reader is referred to the web version of this article.)

is controlled using a Julabo FP51-SI refrigerated circulator. Heat is supplied to the alternate vertical leg of the system using two sets of electric band heaters. The bottom-most set of heaters (labelled *ch* in Fig. 2) is used to generate a steady base flow in the system. The set is used to generate up to 1500 W of heating, and is kept at a fixed vertical position. The top-most set of heaters (labelled *mh*) is used to drive the system to an oscillatory state. The six electric band heaters (up to 11.1 W/cm<sup>2</sup>) are clamped to the system at fixed intervals and can be manually repositioned along the vertical riser between measurements to vary the natural driving height  $\Delta z$  of the NCL and provide up to 2100 W of heating in total. As the flow in a natural circulation loop is driven by a difference in density between the two vertical legs over  $\Delta z$ , the movement of the heaters affects the resulting mean mass flow rate of the system. Furthermore, as all heat exchangers are positioned along the vertical sections of the natural circulation loop, its vertical line symmetry is broken. As such, a preferential counter-clockwise flow direction prevails as shown in Fig. 2. Additionally, in order to minimize heat losses to the surroundings, the NCL is insulated with a 40 mm thick annulus of rockwool insulation. The mass flow rate of the loop can be controlled with a regulating needle valve that introduces an adjustable local pressure drop. The control valve is positioned directly after the cooler. As indicated in green in Fig. 2, the valve can be removed from the loop. Additionally, the volume of the system can be varied using a 1 l piston accumulator, allowing for a maximum volumetric increase of 29% of the NCL. In the accumulator, which is indicated with *accu.* in Fig. 2, nitrogen is used as the compressible secondary medium.

#### 2.1.2. Instrumentation

Several quantities are continuously measured throughout the facility. At eight locations around the loop, a temperature is measured. At  $T_{01}$ ,  $T_{02}$ ,  $T_{03}$  and  $T_{04}$  (as indicated in Fig. 2) the temperature of the

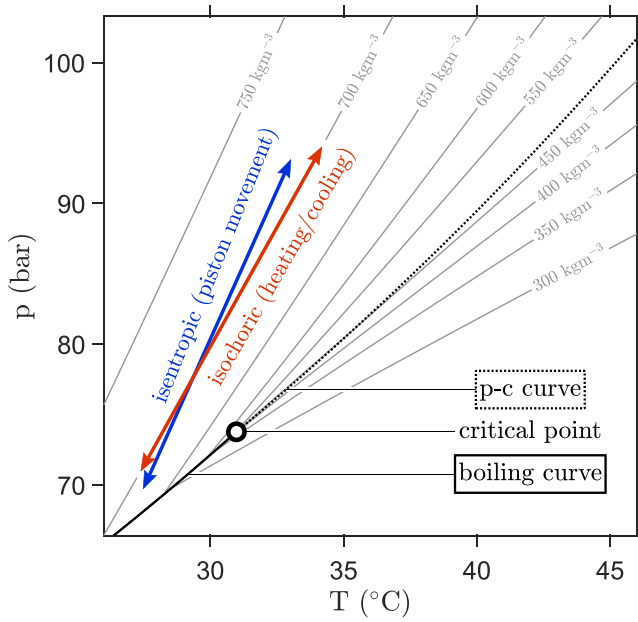


**Fig. 3.** Modes of modulation of the thermodynamic state of the system. During normal operation, the system operates with a constant volume. Under such conditions, any imbalance in heat induces movement of the mean thermodynamic state along a set isochor, as indicated with the red arrow. Any movement of the piston within the accumulator, if connected to the main loop, induces the compression or expansion of the CO<sub>2</sub>. The consequent changes in thermodynamic state are indicated in blue if this process is isentropic. (For interpretation of the references to colour in this figure legend, the reader is referred to the web version of this article.)

CO<sub>2</sub> is directly measured. Here, cylindrical Pt100 thermometers with a 3 mm diameter and a nominal accuracy of  $\pm 0.1$  °C are inserted radially into the flow. A similar arrangement with the same resistance temperature transmitters is used to evaluate the coolant inlet temperature  $T_{c,i}$  and the coolant outlet temperature  $T_{c,e}$ , respectively. The external pipe surface temperature is measured at two points directly above the movable heaters with sensors  $T_{w1}$  and  $T_{w2}$ . Similarly, Pt100 thermometers with a nominal accuracy of  $\pm 0.1$  °C are used. Measurements of the absolute pressure  $p$  are taken using welded STS ATM.1st sensors  $P_{01}$  and  $P_{02}$ , with a nominal uncertainty of  $\pm 0.16$  bar or 0.1%. The mass flow of the loop is measured with a Rheonik RHM08 Coriolis mass flow meter with a nominal uncertainty of 0.2%, at up to 0.2 g/s. If the mass flow meter is removed from the NCL, the mass flow rate ( $\dot{m}_{est}$ ) is estimated from an energy balance over the heaters:

$$\dot{m}_{est} = \frac{\dot{Q}}{h_{out} - h_{in}}, \quad \begin{matrix} h_{out} = h(P_{01}, T_{01}) \\ h_{in} = h(P_{02}, T_{04}) \end{matrix} \quad (1)$$

There,  $h_{in}$  and  $h_{out}$  describe the enthalpy at the in- and outlet of the movable heaters. To minimize errors in  $\dot{m}_{est}$ , both the heating losses and the viscous losses are minimized by insulating the loop and reducing the system mass flow rate, respectively. Since heat losses throughout the system are not currently accounted for, the mass flow rate is overpredicted by Eq. (1). A comparison between steady-state readings from the Coriolis mass flow meter and the estimated mass flow rate  $\dot{m}_{est}$ , for the results of [28] with the current experimental facility, showed that  $\dot{m}_{est}$  exceeded the measured value by  $7.1 \pm 4.0\%$ . All transducer data are acquired at up to 10 Hz using a NI cRIO-9074. The NCL is operated through a Labview user-interface.

### 2.1.3. Modulation of thermodynamic state

The supercritical thermodynamic region of CO<sub>2</sub> in the NCL is explored through either isochoric or isentropic processes, as illustrated in Fig. 3. Isochoric operation is achieved by disconnecting the accumulator, whereby the volume and the contained mass of CO<sub>2</sub> determine

the isochor. Any heat imbalance, caused by changes in heating power or coolant temperature, shifts the thermodynamic state of the system towards a new equilibrium along an isochor, as shown by the red arrow in Fig. 3. Conversely, when the piston accumulator is connected, altering the nitrogen charge compresses or expands the CO<sub>2</sub> in the system. If these changes are adiabatic and with negligible viscous losses, they result in isentropic shifts in the thermodynamic state, as indicated by the blue arrow in Fig. 3.

### 2.1.4. Oscillation trigger procedure

To incite oscillations in the natural circulation loop, the system is first brought to a stable, non oscillatory state. At a given filling mass, the system pressure is increased to beyond 100 bar. Fig. 3 shows the corresponding temperature for a selection of isochors. During this process, only the circulation heaters ( $ch$  in Fig. 2) are active to ensure stability of the system. Once a steady and stable circulation is achieved, the circulation heaters are disconnected, and the movable heaters are enabled. Consequently, the mass flow rate decreases, and the temperature difference between the two vertical legs increases. Thereafter, changes in the coolant temperature may lead to oscillatory behaviour in the natural circulation loop.

### 2.2. One-dimensional static model

Using a static model of the heat exchangers in particular, the system is examined for the presence of multiple steady states. In a static model, both the driving pressure and the viscous pressure loss are expressed as a function of the mass flow rate  $\dot{m}$ . Much like under forced convection, the flow through the NCL heat exchangers is assumed to be driven by constant pressure gradients, independent of the mass flow rate. Then, the criterion for multiple intersections with the viscous pressure loss is

$$\frac{\partial \Delta p_v(\dot{m})}{\partial \dot{m}} < 0, \quad (2)$$

consistent with Swapnalee et al. [21] and Rai et al. [14]. Essentially, the NCL is statically unstable when its viscous losses decrease as the mass flow rate increases. In the unheated sections of the NCL the flow of CO<sub>2</sub> has constant thermophysical properties, and therefore approaches an ideal sub-critical adiabatic flow. However, ideal friction models for sub-critical fluids do not satisfy the criterion of Eq. (2), as their friction factors  $f$  are weak functions of  $\dot{m}$ . On the contrary, when a flow of CO<sub>2</sub> is heated or cooled at a supercritical pressure, its viscous friction may depend strongly on buoyancy and property variations [29–31] and therefore vary significantly from an ideal approximation. It is only under such conditions, that the criterion in Eq. (2) may be satisfied. Therefore, only the heat exchangers of the NCL are expected to be susceptible to static instability, if sufficiently non-ideal.

The following paragraphs present a simplistic one-dimensional model of the viscous losses in the heat exchangers of the current system that qualitatively and phenomenologically captures the effects of variations in several thermophysical properties to a variable extent. Using the model, the degree of non-ideality within the heat exchangers can be varied and compared to existing viscous models to evaluate the susceptibility of the system to static instabilities.

#### 2.2.1. Heat exchanger model

A one-dimensional model is used to approximate the viscous losses  $\Delta p_v$  within the heat exchangers of the supercritical NCL. Fig. 4 shows the numerical grid along which the heat exchangers are discretized with  $N$  elements with lengths  $L$ . Here, nodes  $[0, N]$  span the full length of the heat exchanger. At node 0, the mass flow rate  $\dot{m}$ , the pressure  $p$  and the bulk enthalpy  $h_b$  are imposed. For the successive nodes  $i$ , the bulk enthalpy is determined using

$$h_{b(i)} = h_{b(i-1)} \pm \frac{\dot{Q}}{\dot{m}N}, \quad (3)$$

**Table 2**

Overview of the operating conditions of the current experiments. “valve” and “accu.” indicate the inclusion of the cold-leg valve and the piston accumulator, respectively. If the column under “valve” lists ×, the Coriolis mass flow meter is also excluded from the facility.

Varied par.	Sect.	$\Delta z$ (m)	$\bar{\rho}$ (kgm <sup>-3</sup> )	$\dot{Q}$ (kW)	$\bar{p}$ (bar)	valve	accu.
full range	3	$0.4 \leq \Delta z \leq 2.5$	$450 \leq \rho \leq 750$	$0.8 \leq \dot{Q} \leq 2.0$	$p_c < p < 110$	✓/×	✓/×
case 1	3.1	0.4	700	2.0	$p_c < p < 80$	×	×
case 2	3.1	0.9	700	0.8	$p_c < p < 80$	×	×
driving height	3.2.2	$0.4 \leq \Delta z \leq 0.9$	700	$1.0 \leq \dot{Q} \leq 2.0$	$p_c < p < 110$	×	×
resistance	3.2.3	0.4	700	2.0	$p_c < p < 100$	✓	×
density	3.2.4	0.4	$450 \leq \rho \leq 750$	2.0	$p_c < p < 100$	×	×
heating rate	3.2.5	0.4	700	$1.0 \leq \dot{Q} \leq 2.0$	$p_c < p < 80$	×	×
pressure	3.2.6	0.4	700	2.0	$p_c < p < 110$	×	×
accumulator	3.2.7	0.4	700	2.0	$p_c < p < 80$	×	✓

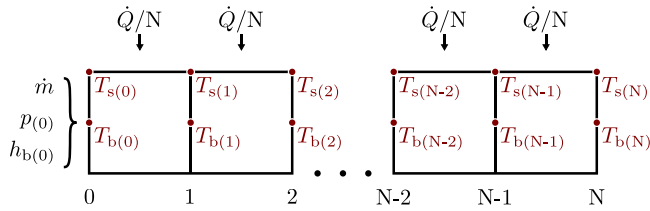


**Fig. 4.** Schematic of static 1-D model of viscous pressure drop  $p_v(\dot{m})$ . The CO<sub>2</sub> temperature is evaluated at the bulk ( $T_b$ ) and the surface ( $T_s$ ) for all  $N$  cells.

where  $\dot{Q}$  is the heating rate. The sign of  $\pm$  depends on whether the movable heaters (+) are considered, or whether the cooler (−) is modelled. The viscous loss for each cell can be estimated using

$$\Delta p_{v(i)} = \frac{(f \dot{m}^2) L}{2 \rho_{b(i-1)} A_{cs}^2 D}, \text{ where } f = f_{ni} \cdot f_{iso}. \quad (4)$$

Here,  $A_{cs}$  is the cross-sectional area of the heat exchanger with inner diameter  $D$  and length  $L$ . The friction factor  $f$  is a multiplication of the ideal and isothermal friction factor  $f_{iso}$  and a coefficient of non-ideality  $f_{ni}$ . The values of  $f_{iso}$  and  $f_{ni}$  are discussed in Section 2.2.2. Using the pressure drop  $\Delta p_{v(i)}$  and bulk enthalpy  $h_{b(i)}$ , the thermophysical properties of node  $i$  can be evaluated as

$$T_{b(i)}, \rho_{b(i)}, \mu_{b(i)} = f \left( h_{b(i)}, p_{(0)} - \sum_0^i \Delta p_{v(i)} \right), \quad (5)$$

The bulk Reynolds number  $Re_{b(i)}$ , for the evaluation of  $f_{iso}$ , is then obtained with

$$Re_{b(i)} = \frac{\dot{m} D}{\mu_{b(i)} A_{cs}}. \quad (6)$$

Here,  $\mu_{b(i)}$  is the bulk viscosity of node  $i$ . As will be elaborated on in Section 2.2.2,  $f_{ni}$  is evaluated with material properties with the wall temperature  $T_{s(i)}$ , which can be determined with

$$T_{s(i)} = T_{b(i)} \pm \frac{\dot{Q}}{A_p U}. \quad (7)$$

Here,  $A_p$  is the surface area of the heat exchanger pipe, and  $U$  is the equivalent heat transfer coefficient. To isolate the effect of viscous losses on the static stability, the current model assumes a constant heat transfer coefficient with a value of  $U = 5 \text{ kWm}^{-2}\text{K}^{-1}$ . The chosen value of  $U$  is within the same order of magnitude as most proposed heat transfer correlations for the present configuration [30,32–35], among which there is large variability. The currently chosen and relatively low value of  $U$  ensures a sufficient temperature difference between the pipe surface and the bulk to emphasize the influence of property variation on the viscous losses.

### 2.2.2. Viscous models

The viscous drag in the loop is modelled using an ideal-fluid model  $f_{iso}$ , and a correction factor  $f_{ni}$  that considers non-ideal effects, as per

**Table 3**

Value of terms in  $f_{ni}$  for current heat exchanger configurations.

Configuration	$\left(\frac{\rho_w}{\rho_b}\right)^\alpha$	$\left(\frac{\mu_w}{\mu_b}\right)^\beta$
cooled downward flow	> 1	> 1
heated upward flow	> 1	< 1

Eq. (4). When non-ideal effects are not considered,  $f_{ni} = 1$ . The Blasius friction law for smooth pipe flows is used to determine  $f_{iso}$ , with

$$f_{iso} = 0.3164 \cdot Re_b^{-1/4}, \quad Re_b < 10^5 \quad (8)$$

The non-ideality caused by non-linear variations in thermophysical properties is approximated using a model that is based on the correlation proposed by Petrov and Popov [36]. This revised friction model is given as

$$f_{ni} = \left(\frac{\rho_w}{\rho_b}\right)^\alpha \left(\frac{\mu_w}{\mu_b}\right)^\beta. \quad (9)$$

Eq. (9) qualitatively considers both the modulation of near-wall velocity by the strong dilation of CO<sub>2</sub> [30,37,38] through  $(\rho_w/\rho_b)$ , and the variation in the near-wall viscosity through  $(\mu_w/\mu_b)$ .

Phenomenologically, when the CO<sub>2</sub> is heated, density decreases at the wall. In an upward heated flow, the buoyancy increases the near-wall velocity, resulting in a stronger shear rate. To capture this effect with  $f_{ni}$ , the exponent  $\alpha$  must be negative. Conversely, in a downward cooled flow, the density increases near the wall, yet buoyancy continues to aid the near-wall flow, similarly leading to a stronger shear rate. Thus, for a cooled downward flow,  $\alpha$  should be positive.

In contrast, the modulation of the friction factor by viscosity is independent of the flow direction. When supercritical CO<sub>2</sub> is heated, the viscosity decreases, reducing the wall shear stress and thereby lowering the friction factor. The opposite is true for the cooler, where the near-wall viscosity is increasing, resulting in a higher friction factor. Consequently,  $\beta > 0$  applies to both heat exchangers.

Thus, the effects of buoyancy and viscosity compete only in the heated upward flow, while in the cooled downward flow both effects increase  $f_{ni} > 1$ , as summarized in Table 3. This has a significant implication for the heater: when  $f_{ni} \ll 1$  the overall friction factor can decrease with increasing mass flow rate to satisfy the criterion in Eq. (2).

It is important to note that turbulence further complicates the modulation of the friction factor. In an upward heated flow, turbulence may weaken due to buoyancy effects and the thermal expansion of the near-wall fluid [33,38], leading to an even greater reduction in the friction factor. This phenomenon, known as heat transfer deterioration, occurs when reduced turbulence results in a lower turbulent heat transfer rate. We have incorporated this effect indirectly when specifying the values for  $\alpha$  and  $\beta$  in Section 4.

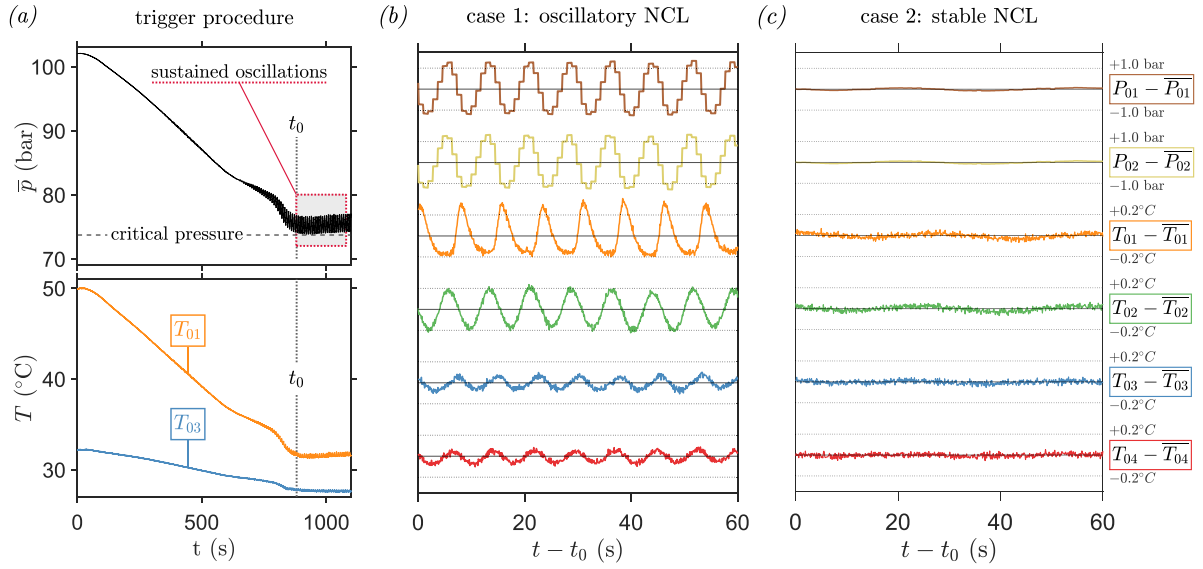


**Fig. 5.** Sustained dynamic oscillations in the supercritical carbon dioxide natural circulation loop. (a) shows the phase leading up to the onset of oscillations in the system. At  $t = 0$  s, the temperature of the coolant is reduced, and the pressure of the initially steady system decreases along an isochor. Subsequently, the system displays finite oscillations in both temperature and pressure, at a mean absolute pressure  $\bar{p} = 76$  bar and nominal density  $\rho = 700 \text{ kg m}^{-3}$ . (b) and (c) compare the normalized signal of several transmitters throughout the system for a case in which the NCL is oscillatory (b) to a case in which the NCL is stable (c), corresponding to case 1 and case 2 of Table 2, respectively. The y-axis values of both (b) and (c) are given in (c).

### 3. Results

The susceptibility of a supercritical pressure NCL to unwanted oscillations is investigated by considering the parameter range given in grey in Table 2. To characterize the instabilities that can occur, the behaviour of the NCL is compared for two distinct conditions within the considered range in Section 3.1. Thereafter, in Section 3.2, the operating conditions and inputs of the NCL are independently varied to assess the validity of existing stability models and to propose oscillation mitigation measures in Section 3.3. The operating conditions and the varied parameters for each of the sections hereafter are indicated in Table 2.

#### 3.1. Overall characterization of the observed NCL instabilities

Starting from the initial steady state described in Section 2.1.4, a decrease in the coolant inlet temperature leads to increased cooling. As a result, the pressure decreases towards the critical pressure. For case 2 of Table 2, the circulation loop remains stable upon this perturbation, and only produces low amplitude and low frequency fluctuations with a period of approximately 37 s. As shown in Fig. 5(c), the fluctuations of the stable NCL only slightly exceed the amplitude of the sensor noise for case 2. The oscillations are caused by periodic corrections of the coolant inlet temperature by the controller of the refrigerated circulator, as will be briefly elaborated in the paragraph hereafter. As the moderate fluctuations are only the consequence of the applied external forcing by the cooler, the system is considered stable.

Conversely, for case 1 of Table 2, sustained oscillations eventually occur when the system is disturbed. As illustrated in Fig. 5(a), a rapid increase in the oscillation amplitude is observed below a mean pressure of  $\bar{P} = 80$  bar. Subsequently, the pressure decreases quickly along the current isochor until the thermodynamic state stabilizes at a mean pressure of  $\bar{P} = 76$  bar. At this new 'equilibrium,' the natural circulation loop exhibits oscillations in temperature and pressure with constant amplitude and frequency, as shown in Fig. 5(b) for a selection of pressure and temperature sensors along the loop.

Under oscillatory conditions, the natural circulation loop is characterized by system-wide signal fluctuations of a larger amplitude and higher frequency than during stable conditions. As shown in Fig.

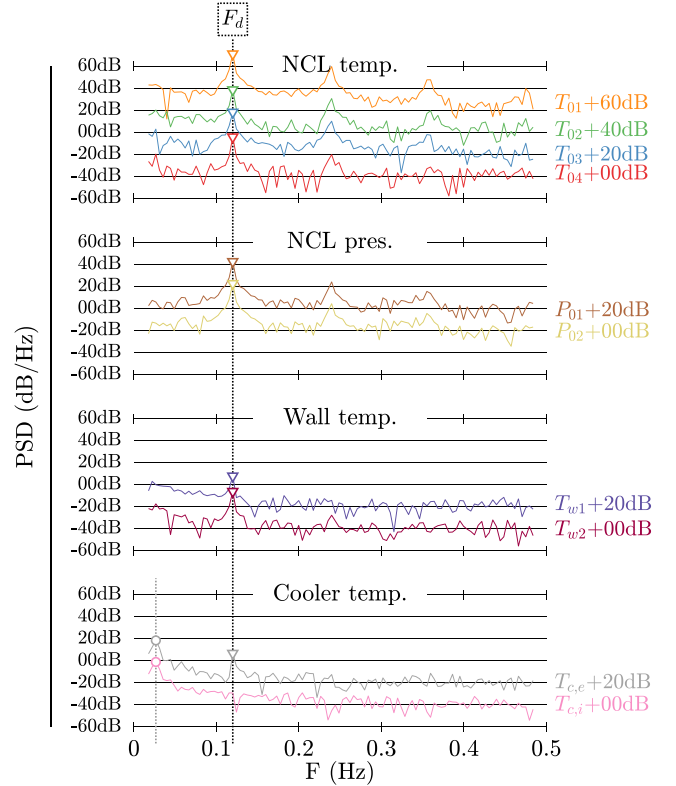


**Fig. 6.** Power spectra of sensor data under oscillatory conditions (case 1 of Table 2). Maxima in the spectra for internal temperature data (NCL temp.), absolute pressure data (NCL pres.) and external wall temperature data (Wall temp.) are indicated with  $\nabla$ . The locations of  $\nabla$  coincide on dominant frequency  $F_d$ . Maxima in the spectra of the coolant temperatures (Cooler temp.) are indicated with  $\circ$ , and with the grey dotted line. An additional local maximum in the spectrum of cooler outlet temperature  $T_{c,e}$  is indicated with  $\nabla$ .

5(b), the respective signals vary in amplitude and phase when the system is in an oscillatory state. However, as can be deduced from Fig. 6, all primary loop oscillations have the same dominant frequency. Fig. 6 shows the power spectra of all sensors for a single case, and indicates their global peaks. For the loop temperature, pressure, and wall temperature data the global maxima are indicated with  $\nabla$ . For these sensors, the global spectrum maxima coincide at  $F_d$ . Therewith, the oscillations in temperature and pressure are assumed to originate from the same phenomenon, despite their respective phase lags. For coolant sensors  $T_{c,i}$  and  $T_{c,e}$ , the global maximum is indicated with  $\circ$ . The frequency at which  $T_{c,i}$  and  $T_{c,e}$  oscillate is significantly lower than for the other sensors in the system, and coincides with the frequency at which the coolant temperature is controlled. It is also this frequency that drives the moderate oscillations seen during the steady operation of the loop, as shown in Fig. 5(c).

The natural circulation loop displays both synchronized and non-synchronized fluctuations when it is oscillating. In line with case 2 of Fig. 5(c), the fluctuations in temperature are always out of phase. There, the relative phase lag between the temperature signals varies among the experiments. In Fig. 7, the respective phase lags of the temperature signals of case 1 of Table 2 are shown in a space-time diagram. The figure indicates an approximation of the local circulation velocities in both the hot- and cold sections of the system,  $U_h$  and  $U_c$ , with

$$U_h = \frac{\dot{m}_{est}}{\rho_h \frac{\pi}{4} D^2}, \quad \rho_h = \rho \left( P_{01}, \frac{T_{01}}{2} + \frac{T_{02}}{2} \right), \quad (10)$$

and

$$U_c = \frac{\dot{m}_{est}}{\rho_c \frac{\pi}{4} D^2}, \quad \rho_c = \rho \left( P_{02}, \frac{T_{03}}{2} + \frac{T_{04}}{2} \right). \quad (11)$$

There, the advection velocities are assessed using the estimated mass flow rate  $\dot{m}_{est}$ , and the densities for the hot- and cold sections  $\rho_h$  and  $\rho_c$ . In Fig. 7, lines of  $U_h$  and  $U_c$  are superimposed upon the temperature signals. These lines are drawn for every period  $1/F_d$ , the period of the dominant oscillation of case 1. In the figure, lines of constant  $U_h$  that intersect the signal of  $T_{01}$  at a wave crest also intersect a subsequent wave crest of  $T_{02}$ . Similarly, lines of constant  $U_c$  intersect fluctuation crests of both  $T_{03}$  and  $T_{04}$ . Therewith, Fig. 7 suggests the presence of thermal waves that are advected through the natural circulation loop at the local circulation velocity. Then, the relative phase lags of oscillations at the temperature sensors vary as the mass flow rate of the system changes. On the contrary, the pressure oscillations are always in phase within the considered parameter range. This synchronization of the pressure signals suggests the occurrence of a global thermal (de)compression of the system, upon which the pressure is redistributed almost instantaneously at the local speed of sound. When heat is transferred to- or from the loop, the pressure of the system varies along the red isochoric arrow in Fig. 3. However, as the thermal diffusivity and the mixing of the carbon dioxide is finite, the temperature of the  $\text{CO}_2$  is not redistributed instantaneously. Instead, the temperature of the  $\text{CO}_2$  near the source of the heat imbalance builds, and a ‘pocket’ of carbon dioxide with a different density than the fluid it is surrounded by is formed. As these thermal pockets are then advected by the flow, they assume the form of the currently observed thermal fluctuations, and induce system-wide oscillations.

### 3.2. Sensitivity to operating parameters

To explore the stability boundary between the oscillations in case 1, and the steady circulation of case 2, the operating parameters of the NCL are varied independently hereafter. Therewith, we aim to approach and cross the most widely accepted stability boundaries of supercritical pressure NCLs proposed by Debrah et al. [13], Ambrosini and Sharabi [15] in experiment. The operating conditions and independently varied parameters for each of the subsections hereafter are given in Table 2.

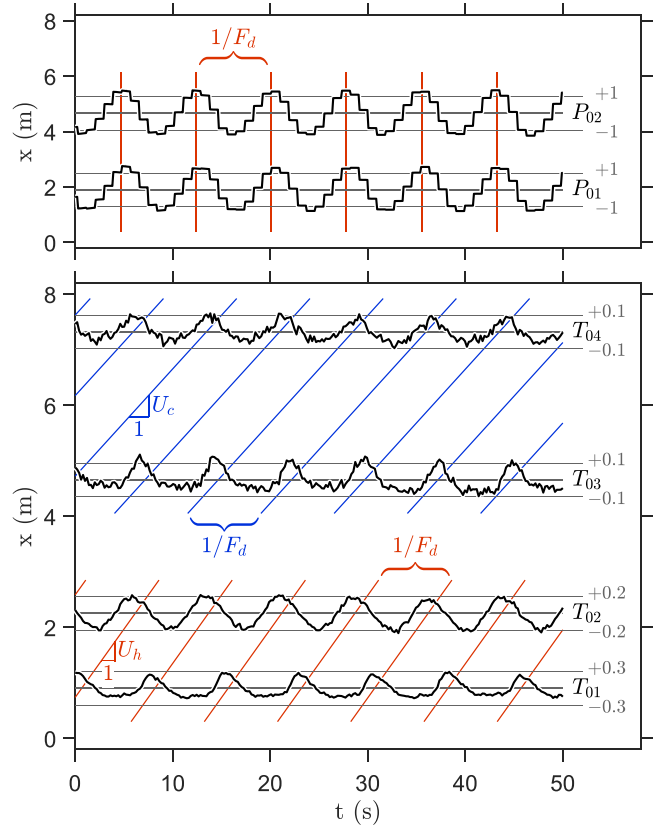


Fig. 7. Space-time comparison of respective phase lag of NCL signals with respect to the dominant frequency  $F_d$  and the hot- and cold leg advection velocities  $U_h$  and  $U_c$ , respectively. For the case shown in the figure (case 1 of Table 2),  $\dot{m}_{exp} = 48.2 \text{ gs}^{-1}$ ,  $U_h = 0.25 \text{ ms}^{-1}$ , and  $U_c = 0.19 \text{ ms}^{-1}$ . The normalized values of the sensor outputs are shown at their respective positions  $x$  along the loop.

#### 3.2.1. Stability map

Based on the linearized one-dimensional numerical analysis of the supercritical pressure NCL, Debrah et al. [13], Ambrosini and Sharabi [15] have proposed maps of the stability of the current system. The stability boundaries of the NCL are expressed using dimensionless quantities  $N_{SUBPC}$  and  $N_{TPC}$ , with

$$N_{SUBPC} = \frac{\beta_{pc}}{C_{p,pc}} (h_{pc} - h_{b,h}), \quad N_{TPC} = \frac{\beta_{pc}}{C_{p,pc}} \frac{\dot{Q}}{\dot{m}}. \quad (12)$$

In Eq. (12),  $\beta_{pc}$ ,  $C_{p,pc}$  and  $h_{pc}$  are the volumetric coefficient of thermal expansion, the specific heat and the enthalpy of  $\text{CO}_2$  at the p-c curve for the considered pressure, respectively. Furthermore,  $h_{b,h}$  is the bulk enthalpy at the heater inlet. Dimensionless parameter  $N_{SUBPC}$  quantifies the relative distance of the operating point to the pseudo-critical line at the current pressure, or the degree of pseudo sub-cooling. At  $N_{SUBPC} = 0$ , the heater inlet flow would be at pseudo-critical temperature.  $N_{TPC}$  conveys the extent of the energy exchange with the  $\text{CO}_2$  relative to the energy rate initially present in the flow. Effectively,  $N_{TPC}$  communicates the relative change in energy of the medium through the heat exchangers. Debrah et al. [13], Ambrosini and Sharabi [15] predict that beyond a certain value of  $N_{TPC}$ , where the thermophysical properties of the  $\text{CO}_2$  change dramatically within the heat exchangers, the system is prone to unstable behaviour.

In the sections that follow,  $N_{TPC}$  and  $N_{SUBPC}$  are varied by adjusting the operating conditions and input parameters of the experimental facility to approach the stability boundaries discussed above.

#### 3.2.2. Driving height ( $\Delta z$ )

To increase  $N_{TPC}$  towards the predicted boundaries of stability at a given thermodynamic point, either  $\dot{Q}$  should be increased or  $\dot{m}$

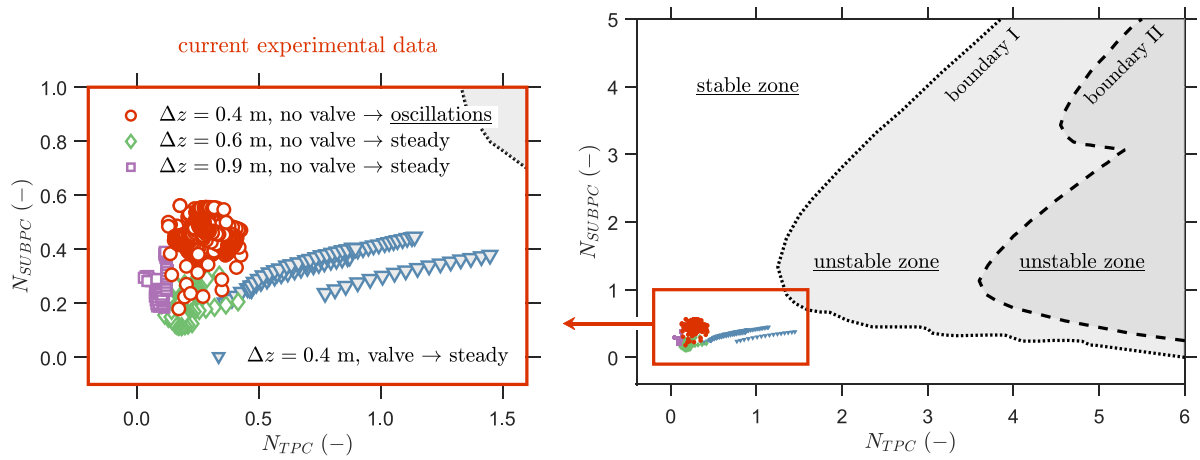


Fig. 8. Non-dimensionalized parameter space map. The current experimental data is compared to the linear stability maps presented in Debrah et al. [13] (boundary I) and Ambrosini and Sharabi [15] (boundary II).

should be decreased. As the available heating rate  $\dot{Q}$  is limited in the current facility,  $\dot{m}$  was varied instead to substantially increase  $N_{TPC}$ . In this work, the mass flow rate of an NCL with a set diameter is independently decreased either by decreasing  $\Delta z$ , or by increasing the frictional resistance of the system by introducing a local loss.

The current section discusses the influence of reducing the mass flow rate  $\dot{m}$  solely by varying  $\Delta z$ . The sensitivity to the inclusion of local resistances is discussed in Section 3.2.3. To vary  $\Delta z$  in the current experiments, the moveable heaters ( $mh$  in Fig. 2) are moved vertically to impose various driving heights. Currently, driving heights of  $\Delta z = 0.4, 0.6$ , and  $0.9$  m are considered. Fig. 8 shows the present experimental data in comparison with the stability maps presented in Debrah et al. [13], Ambrosini and Sharabi [15]. As  $\Delta z$  is decreased, the mean value of  $N_{TPC}$  increases. Eventually, when  $\Delta z$  is reduced to  $0.4$  m, oscillatory behaviour is perceived throughout the system. For  $\Delta z = 0.6$  or  $0.9$  m, a steady circulation results from the operation of the supercritical NCL. Therefore, in qualitative agreement with the linear stability maps shown in Fig. 8, increasing  $\dot{m}$  by increasing  $\Delta z$  suppresses oscillations. However, the current limits of stability do not directly coincide with the numerically predicted boundaries. The present experiments show oscillations at lower values of  $N_{TPC}$ , outside of the unstable regions of Fig. 8. Therefore, a departure from stability of supercritical NCLs may occur before the predicted one-dimensional model limits are reached under the current conditions.

### 3.2.3. Local resistance (valve)

By including a local resistance to the natural circulation loop to reduce its mass flow rate, the system becomes stable. With a regulating valve in the NCL's cold section (immediately downstream of the cooler in Fig. 2), no oscillations could be induced in the system, regardless of the degree to which the valve was opened. Similarly, placing the Coriolis mass flow meter in the cold leg (below the valve in Fig. 2) prevented oscillations. As such, sustained oscillations were only observed when no resistive elements or flow obstructions were present. Therefore, the cold-side valve and the mass flow meter (both outlined in green in Fig. 2) were removed from the system for all other sensitivity experiments in this work.

The sensitivity of the NCL's transient to a local resistance highlights limitations to the established descriptions of the stability boundary, in which the boundary is only expressed using  $N_{TPC}$  and  $N_{SUBPC}$ . The experiments without resistive elements match the predicted trend in  $N_{TPC}$  qualitatively: a decrease in  $\Delta z$  increases  $N_{TPC}$  to a threshold value beyond which the natural circulation loop is no longer steady. However, as can be seen in Fig. 8, stability is maintained at significantly higher values of  $N_{TPC}$  upon the inclusion of a cold leg valve for the same driving height. Therewith, whereas the inclusion of a local

resistance reduces the mass flow rate  $\dot{m}$  effectively to increase  $N_{TPC}$ , it also affects the stability of the loop. Therefore, an additional parameter beyond  $N_{TPC}$  and  $N_{SUBPC}$  that takes into account the increased friction or mixing by the local resistance should be considered to describe the stability boundary of the supercritical pressure NCL.

### 3.2.4. Density ( $\rho$ )

The degree of pseudo-sub-cooling affects the stability of the system and the relative amplitude of the oscillations in the NCL. In this work, the density of the  $\text{CO}_2$  is varied to change the degree of pseudo-sub-cooling, considering  $450 \leq \bar{\rho} \leq 750 \text{ kgm}^{-3}$ . Fig. 9 highlights the evolution of the oscillations along two distinct isochors within this parameter space. The two isochors are chosen such that the outlet conditions of either one of the two heat exchangers are in the direct vicinity of the pseudo-critical curve. At  $\times$  in the figure, the oscillations are incited similarly to Fig. 5(a).

In Fig. 9(a), an oscillatory case with a mean NCL density of  $\bar{\rho} = 700 \text{ kgm}^{-3}$  is considered. The figure shows the evolution of the fluctuations in temperature and pressure for the hot ( $T_{01}, P_{01}$ ) and cold ( $T_{03}, P_{02}$ ) sections of the loop, respectively. For the current isochor the heater outlet temperature  $T_{01}$  approaches the p-c curve. Under these conditions, the  $\text{CO}_2$  is liquid-like, expanding rapidly upon its heating. Large oscillations arise from the non-ideal heater, propagating through the system to the cold leg, in accordance with Fig. 5(b). The thermodynamic range within which these system-wide oscillations are perceived for the current experiments is indicated using the coloured areas of Fig. 9(a). All data presented in this work, apart from the data shown in Fig. 9(b), were recorded within the indicated coloured region.

When the system density is reduced to  $\bar{\rho} = 450 \text{ kgm}^{-3}$ , the NCL is less susceptible to oscillations. Fig. 9(b) shows a typical attempt to incite oscillations in the natural circulation loop, consistent with the methods used for Figs. 9(a) and 5(a). At the conditions of Fig. 9(b), the  $\text{CO}_2$  is cooled towards (and across) the p-c curve. The magnitude of the fluctuations – if at all present – do not exceed the measurement noise of the sensors at  $p \geq 80$  bar. Below  $80$  bar, when the  $\text{CO}_2$  is sufficiently non-ideal in the vicinity of the p-c curve at near-critical pressures, finite oscillations do appear. However, these oscillations are confined to the hot leg of the supercritical NCL, as is shown by the orange-outlined insert of Fig. 9(b). None of the current experiments show oscillations limited only to the cold section of the circulation loop.

As the density is changed from  $700 \text{ kgm}^{-3}$  to  $450 \text{ kgm}^{-3}$ ,  $N_{SUBPC}$  is reduced to a near-zero value. The consequent stabilization of the system is therefore in qualitative agreement with the stability maps proposed by Debrah et al. [13], Ambrosini and Sharabi [15], which show an increased boundary value for  $N_{TPC}$  as  $N_{SUBPC}$  converges to zero.

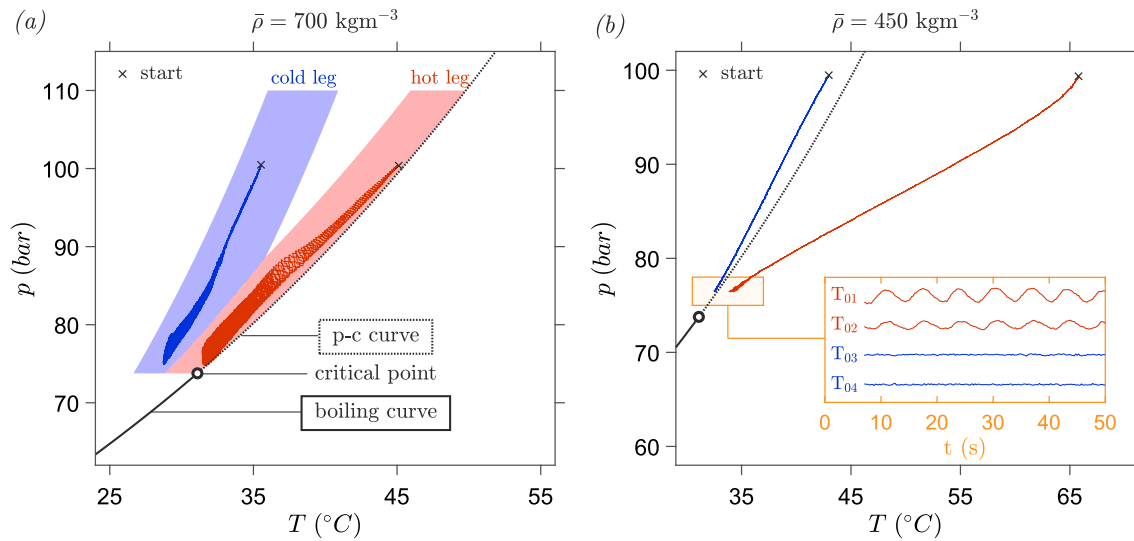


**Fig. 9.** Example of oscillations in the hot leg ( $T_{01}$  &  $P_{01}$ , red) and the cold leg ( $T_{03}$  &  $P_{02}$ , blue) of the NCL at a mean density of (a)  $\bar{\rho} = 700 \text{ kgm}^{-3}$  and (b)  $\bar{\rho} = 450 \text{ kgm}^{-3}$ . (b) highlights the oscillations in  $T_{01}$ - $T_{04}$  for  $\bar{\rho} = 450 \text{ kgm}^{-3}$ . Within (b), the y-scales ranges of  $T_{01}$ - $T_{04}$  are identical. The cases show the growth of dynamic oscillations within the parameter space upon their inception at 100 bar. The coloured region in (a) indicates the thermodynamic region within which the sensitivity of the NCL is evaluated in this work. (For interpretation of the references to colour in this figure legend, the reader is referred to the web version of this article.)

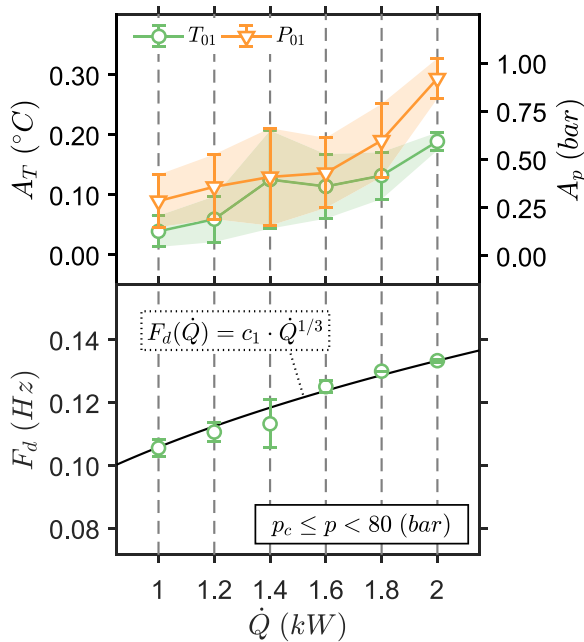


**Fig. 10.** Sensitivity of oscillation amplitude in temperature data of  $T_{01}$  (green, left vertical axis) and pressure data of  $P_{01}$  (orange, right vertical axis) to the imposed heating rate  $\dot{Q}$  in top subfigure. The bottom subfigure shows the sensitivity of the dominant oscillation frequency (evaluated for  $T_{01}$ ) to the imposed heating rate  $\dot{Q}$ . The shaded region and the errorbars indicate the standard deviation ( $\pm\sigma$ ) of the data. (For interpretation of the references to colour in this figure legend, the reader is referred to the web version of this article.)

### 3.2.5. Heating rate ( $\dot{Q}$ )

Changes to the applied heating rate modulate both the amplitude of the measured fluctuations, and their frequency. Fig. 10 shows the evolution of the mean amplitudes  $A_p$  and  $A_T$  in temperature ( $T_{01}$ ) and pressure ( $P_{01}$ ) respectively, and the dominant oscillation frequency  $F_d$  when the heating rate in the heater  $\dot{Q}$  is varied. As the heating rate  $\dot{Q}$  is decreased from  $\dot{Q} = 2 \text{ kW}$ , the value of  $N_{\text{TPC}}$  decreases. Consequently, the oscillation amplitudes decrease accordingly. Within the current parameter range, the amplitudes of the thermal and pressure oscillations

decrease by approximately threefold when the applied heating rate is halved.

Any change in  $\dot{Q}$  is furthermore observed to modulate the mean oscillation frequency throughout the loop, as shown in the bottom panel of Fig. 10 for NCL pressures within  $p_c < p < 80 \text{ bar}$ . As established in Swapnalee et al. [21] and Draskic et al. [28], the mass flow rate of an NCL at a supercritical pressure scales with  $\dot{Q}^{1/3}$ . In Fig. 10, the evolution of  $F_d$  is compared to  $\dot{Q}^{1/3}$ , by including curve  $c_1 \cdot \dot{Q}^{1/3}$ , where the value of  $c_1$  is chosen such that the curve coincides with the mean experimental frequency at  $\dot{Q} = 2 \text{ kW}$ . Within the considered parameter range, the empirical oscillation frequency shows close agreement with the theoretical curve. For these conditions, the frequency of the NCL oscillations is assumed to scale with the mass flow rate of the  $\text{CO}_2$ .

### 3.2.6. Operating pressure ( $p$ )

An increase in operating pressure beyond the critical point increasingly dampens the oscillations in the NCL. Fig. 11 shows the amplitude variations of temperature and pressure along the loop for various imposed pressure ranges. Consistent with the singular cases shown in Figs. 5(a) and 9(a), the mean oscillation amplitudes throughout the loop shown in Fig. 11 decrease as the operating pressure of the system is increased. By increasing the pressure along an isochor, the value of  $N_{\text{SUBPC}}$  decreases, increasing the theoretical boundary value in  $N_{\text{TPC}}$  [13,15]. Therewith, the current data is in qualitative agreement with the predicted stability boundaries. The decrease in oscillation amplitude is most notable in the pressure data for the current experiments. As thermodynamic property gradients decrease with increasing pressures within the considered range (as is shown in Figs. 1(b)–(d)), the non-ideality in the heat exchangers decreases, consequently reducing the magnitude of the oscillations. The dampening of the temperature fluctuations is less apparent. Most notably, the cold-leg temperature amplitudes at  $T_{03}$  and  $T_{04}$  decrease beyond 90 bar. There, the oscillation amplitudes are of an equivalent magnitude as the measurement noise.

The oscillation amplitudes vary with increasing distance away from the heaters. Fig. 11 shows the mean oscillation amplitudes as a function of the streamwise distance from the heater outlet for the respective pressure ranges. In line with case 1 of Table 2 (shown in Fig. 5), the temperature sensor directly downstream of the heater ( $T_{01}$ ) always shows the largest temperature fluctuations in the present study. Therewith, the previous hypothesis of travelling thermal waves is further supported. As the thermal fluctuations are advected away from  $T_{01}$ , they

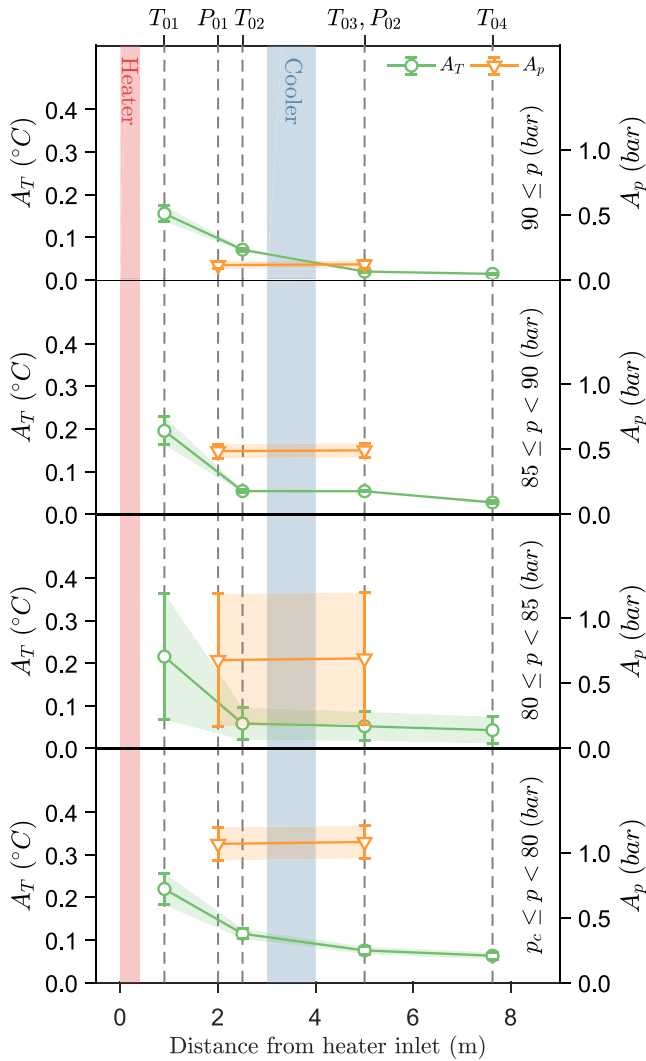


Fig. 11. Mean oscillation amplitudes  $A_T$  of  $T_{01}$ - $T_{04}$  (green, left vertical axis) and  $A_p$  of  $P_{01}$ - $P_{02}$  (orange, right vertical axis), for  $\dot{Q} = 2$  kW. The shaded region and the errorbars indicate the standard deviation ( $\pm\sigma$ ) of the data. (For interpretation of the references to colour in this figure legend, the reader is referred to the web version of this article.)

exchange heat with the thermally inert pipe walls and their surrounding  $\text{CO}_2$ , and experience turbulent mixing. As such, the temperature oscillation amplitudes (in green in Fig. 11) decay with increasing distance from the movable heaters. On the contrary, the pressure amplitude remains constant among  $P_{01}$  and  $P_{02}$ . A constant pressure amplitude is in support of the instantaneous redistribution of pressure resulting from a thermal imbalance of the system, as previously elaborated on in Section 3.1.

### 3.2.7. Accumulator (accu.)

The inclusion of a piston accumulator to the current experiments results in minimal changes to the perceived oscillations. In Fig. 12, the influence of the accumulator on the NCL pressure is considered. Initially, the piston accumulator is connected to the main system which experiences system-wide oscillations similar to those shown in Fig. 5(b). At first, the accumulator contains approximately 0.95 l of compressible  $\text{N}_2$ . At  $t = 256$  s, the  $\text{CO}_2$  level within the accumulator is suddenly increased through the rapid removal of  $\text{N}_2$ . Consequently, the mean pressure of the system decreases quickly along the isentrope indicated in blue in Fig. 3. Thereafter, oscillations of equal frequency as the initial fluctuations emerge, and a new thermodynamic mean state is reached.

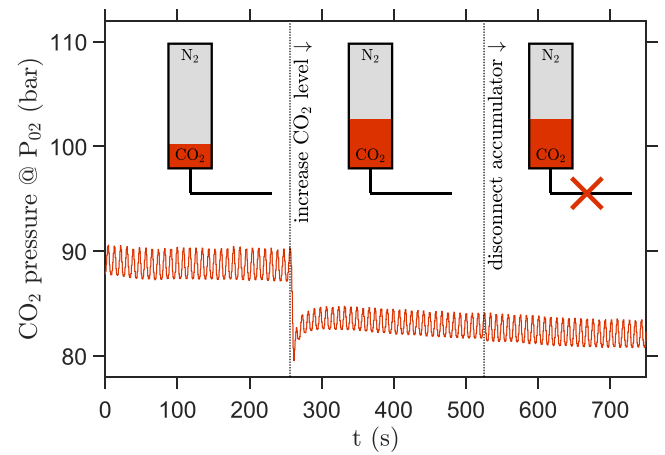


Fig. 12. Typical effect of the movement of the accumulator piston on the oscillations within the NCL. Initially, at and before  $t = 0$  s, the accumulator is connected to an oscillatory loop. At  $t = 256$  s,  $\text{N}_2$  is suddenly removed from the accumulator and the  $\text{CO}_2$  level and vertical piston position consequently increase. At  $t = 525$  s, the ball valve between the accumulator and the NCL is closed, disconnecting the accumulator from the rest of the system.

Subsequently, at  $t = 525$  s, the piston accumulator is disconnected from the NCL by abruptly closing the ball valve connecting the accumulator and the main loop in Fig. 2. As a result, an instantaneous but moderate increase in oscillation amplitude is observed. Nevertheless, the frequency of the oscillations within the NCL remains constant. As such, the presence of a compressible volume has led to negligible modulation of the stability of a supercritical NCL in the current experiments. However, the total accumulator volume with respect to the NCL volume is moderate in the current work. In Huang et al. [22], a much larger accumulator is used than in the current study, with 55 l of  $\text{N}_2$  capacity. The oscillations in their experiments – albeit of a different type than the ones observed in the current study – were strongly affected by the inclusion of a pressurization accumulator.

### 3.3. Instability mitigation measures

The current experiments provide valuable insights into preventing and mitigating prolonged oscillations that can lead to equipment fatigue in high-throughput passive circulators at supercritical pressures. In oscillation-prone environments, narrowing the thermodynamic range that is spanned within the heater eventually stabilizes the supercritical NCL. Effectively, this is achieved by reducing  $N_{\text{TPC}}$ . The value of  $N_{\text{TPC}}$  can be reduced in experiments by increasing the mass flow rate (through an increase in  $\Delta z$ ), or by decreasing  $\dot{Q}$ . Furthermore, the present variation in oscillation amplitudes suggests their dependence on the thermodynamic conditions. Within the considered thermophysical range of  $450 \leq \bar{\rho} \leq 750 \text{ kg m}^{-3}$  and  $73.7 \leq \bar{p} \leq 110.0$  bar, the oscillations were significantly weakened at higher pressures ( $\bar{p} \geq 90$  bar) and lower densities ( $\bar{\rho} \leq 500 \text{ kg m}^{-3}$ ), where the value of  $N_{\text{SUBPC}}$  approached zero. There, the property gradients within the heater are reduced by moving away from the p-c curve to a lower density, or by increasing the pressure. A more substantial stabilization of the system is achieved through the impedance of the travelling thermal waves within the system. If the thermal pockets are diffused within the system, for instance by mixing in a parallel-channel plate heat exchanger [25], they no longer affect the NCL velocity to incite a subsequent pocket, and the oscillations are not sustained. Furthermore, the inclusion of a local resistance (a valve or a mass flow meter) decreases the system's sensitivity to accelerations by the thermal waves, beside inducing additional diffusion by mixing near the valve. Thereafter, the formation of the thermal waves is no longer re-incited.

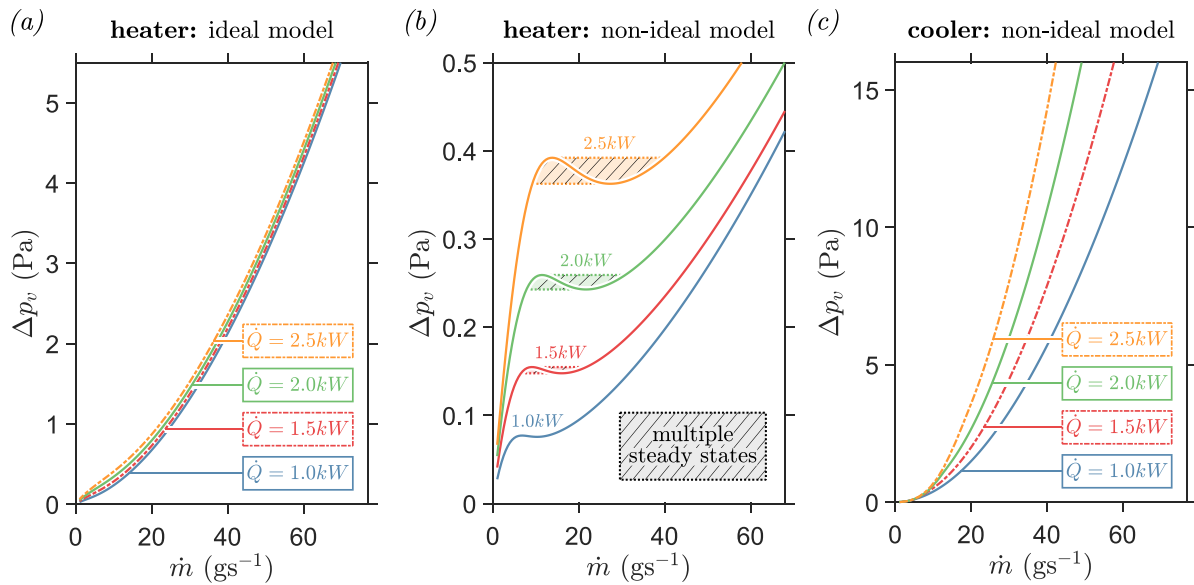


Fig. 13. Steady state analysis of forced flow through movable heaters (*mh*), with inlet pressure  $P_{in} = 80$  bar and inlet bulk density  $\rho_{b,in} = 700 \text{ kgm}^{-3}$ . The values of the viscous drag through the heater, as modelled using an ideal friction model ( $f_{ni} = 1$  in Eq. (4)) or a simplified non-ideal friction model ( $f_{ni}$  from Eq. (9)) are shown in subfigures (a) and (b), respectively. The viscous drag through the cooler, as modelled using an equivalent simplified non-ideal friction model is shown in subfigure (c).

#### 4. Proposed instability mechanism

The observed travelling thermal waves are driven by non-ideality in the heaters. With increasing streamwise distance from the movable heaters in Fig. 10, the amplitude of the temperature oscillations consistently decrease. Within the loop, the oscillations are the strongest directly after the heaters at sensor  $T_{01}$ , regardless of the operating pressure, heating rate and density. Furthermore, the current experiments never show oscillations that are limited only to the cold leg of the NCL. On the contrary, as is shown in Fig. 9, oscillations exclusive to the hot leg do occur. As discussed in Section 3.1, the in-phase pressure oscillations are believed to be induced by the thermal (de)compression of the supercritical pressure  $\text{CO}_2$ . In the heaters, a constant heat flux is electrically applied. For such a constant  $\dot{q}$ , the heat transfer must deteriorate and enhance subsequently to cause the heat imbalance that drives the thermal (de)compression of the system. Upon the deterioration of the heat transfer, heat is removed less effectively from the heater, and the heater wall temperature increases. As the heat transfer is restored thereafter, the  $\text{CO}_2$  is heated at an increased rate, and a low-density ‘pocket’ is formed. At the same time, the system is thermally compressed, increasing the pressure along the current isochor.

The process through which non-ideality is induced in the heaters is not of the static type. Using the steady model introduced in Section 2.2, the static stability of the NCL heat exchangers is assessed. Fig. 13 shows the viscous drag curves of the heat exchangers for several discrete heating rates within the experimentally considered range. As shown in Fig. 13(a), the criterion of Eq. (2) is not satisfied when an ideal viscous model for which  $f_{ni} = 1$  is used within the movable heaters. Then,  $\Delta p_v$  increases progressively for all considered values of  $\dot{Q}$ , and only one steady state exists for a constant driving pressure. However, the criterion of Eq. (2) can be satisfied with a sufficiently non-ideal viscous loss model. Given Eq. (4), the overall friction coefficient  $f$  should scale with  $\dot{m}^\gamma$ , where  $\gamma \leq -2$ , to model viscous losses that decrease as a function of  $\dot{m}$  and therefore satisfy the criterion in Eq. (2). Fig. 13(b) shows a hypothetical viscous loss model for which the heater has multiple steady states. The model assumes  $\alpha = -0.2$  and  $\beta = 3.0$  (satisfying  $\gamma < -2$ ) for  $f_{ni}$  in Eq. (9), for which the modulation of the viscous losses is dominated by the near-wall decrease in viscosity. Given an environment with sufficient perturbations, the steady curves shown in Fig. 13(b) could yield behaviour that is qualitatively similar to the

current oscillations. The limit cycle oscillations between steady states within the hatched areas of Fig. 13(b) would increase in amplitude for increasing heating rates  $\dot{Q}$ , in line with the results of Fig. 10. Additionally, the extension of the model to the cooler with  $\alpha = 0.2$  and  $\beta = 3.0$  (shown in Fig. 13(c)) yields the static stability of the cooler under the same operating conditions, in line with the current experiments in which fluctuations only arise from the movable heaters. However, the values of coefficients  $\alpha$  and  $\beta$  required to achieve a static instability are far beyond what has been empirically reported to date [29–31]. Additionally, the static model of the heater does not change upon the inclusion of the regulating valve, although the stability is greatly affected by the addition of the local resistance in experiment. Therefore, the current oscillations cannot be the direct consequence of only a static instability.

Instead, the non-ideality in the movable heaters is likely triggered by a dynamic feedback mechanism within the system. One such feedback mechanism was proposed by Welander [16] for a sub-critical fluid. There, sustained oscillations arise from the subsequent acceleration and deceleration of the NCL after the formation of thermal waves. A full oscillation cycle is completed when a thermal wave, that is formed by the modulation of the heater residence time, passes through the system. Therewith, the oscillation frequency depends on the mass flow rate of the system. As argued in Section 3.2.5 and with the bottom panel of Fig. 10, the current oscillation frequency scales with the NCL mass flow rate, in support of the mechanism. Furthermore, the present density waves affect the distribution of density within the vertical legs of the NCL, modulating the velocity of the natural circulation. There, a sudden system-wide deceleration of  $\text{CO}_2$  could trigger a deterioration of the heat transfer in the heaters. Subsequently, as the resulting density wave reaches the cold vertical leg, the system accelerates and the heat transfer would recover. Once the density wave reaches the hot leg again, a system-wide deceleration follows, inducing the current cyclic behaviour. Additionally, the inclusion of a local loss reduces the acceleration of the system upon a redistribution of its driving density. Furthermore, the local loss increases mixing, diffusing the travelling thermal wave as it passes. Therewith, the initial conditions for the cyclic deterioration may no longer be met when a valve is present, in line with the current experiments.

## 5. Conclusions

In this study, the stability of a natural circulation loop (NCL) with carbon dioxide at supercritical pressures is experimentally investigated. Such supercritical pressure NCLs offer high-throughput passive circulation without mechanical propulsion, making them highly desirable for cooling in critical applications, including nuclear reactors and solar thermal systems. However, instabilities similar to those seen in two-phase systems can arise in supercritical NCLs at large throughputs, leading to undesirable oscillatory behaviour. Such prolonged oscillations can lead to mechanical fatigue, which is particularly dangerous given the high-pressure environment of supercritical NCLs.

The current work employs an NCL with a vertical-heater-vertical-cooler configuration in which CO<sub>2</sub> is circulated at supercritical pressures. To study the transient of the system, its temperature and pressure are recorded at multiple locations throughout the loop. In search of oscillations, the vertical position of the heaters, the system's thermodynamic state and heating rate, and the presence of a compressible volume or local resistance are varied within the current experiments. Additionally, the experimental results are compared to a static analysis of the NCL to assess whether the potential existence of multiple steady states in the non-ideal heat exchangers in particular drives the recorded fluctuations.

When sufficiently large thermophysical variations are induced in the heat exchangers of the NCL, the loop converges to a system-wide oscillatory state. To reach an oscillatory state in the present study, the mass flow rate of the NCL is decreased by reducing the vertical distance between the cooler and the movable heaters. Then, oscillations are recorded even before the stability limits as predicted by linear one-dimensional analyses are reached. The structural decay in temperature fluctuation amplitudes away from the movable heaters for any of the considered isochors indicates that the fluctuations are initiated at the heaters. The transient heat transfer that occurs in the heaters generates system-wide pressure oscillations, and travelling density waves that manifest as out-of-phase fluctuations in temperature throughout the loop. As the pressure of the system is increased to less non-ideal isobars, the oscillation amplitudes decrease. Conversely, the oscillations intensify at larger heating rates. Furthermore, an increase in heating rate increases the oscillation frequency at a rate equal to the increase in mass flow rate. Qualitatively, the present experiments match the behaviour of a system with multiple steady states. However, as the non-ideality in the heaters that is required to induce multiple steady states under the current conditions exceeds any previous reports, the oscillations are not believed to be incited by a static stability. Instead, the current oscillations are argued to be dynamic. There, the feedback between the heat transfer in the heaters and the velocity of the NCL, modulated by a transient redistribution of density along its vertical legs, is believed to incite the current oscillations. The full stabilization of the system upon the inclusion of a local resistance in its cold leg supports the presence of a dynamic feedback mechanism.

The present work emphasizes the necessity for further investigations into the mechanism that triggers the current Density Wave Oscillations (DWOs). Whereas the current results suggest the presence of a dynamic feedback mechanism, the exact nature of the feedback mechanism is not directly measured in the experiments. A more in-depth understanding of the onset of the current oscillations and their interaction within the NCL could aid in developing effective mitigation strategies that ensure the safe and effective operation of prospective cooling systems of fluids at supercritical pressure. For instance, optical measurements or three-dimensional models of the heaters could aid in predicting the onset of the cyclic deterioration of their heat transfer. Furthermore, the existing non-linear models could be extended to include non-idealities in the heat exchangers and the decay and mixing of the density wave through the system. Additionally, further research on the use of accumulators with a substantial volume relative to the NCL would provide valuable insights into how compressible volumes impact and potentially reduce oscillatory behaviour.

## CRediT authorship contribution statement

**Marko Draskic:** Writing – review & editing, Writing – original draft, Methodology, Investigation, Formal analysis, Data curation, Conceptualization. **Isabelle M.E. Nelissen:** Writing – original draft, Methodology, Investigation, Formal analysis, Data curation. **Rene Pecnik:** Writing – review & editing, Supervision, Project administration, Investigation, Funding acquisition.

## Declaration of competing interest

The authors declare that they have no known competing financial interests or personal relationships that could have appeared to influence the work reported in this paper.

## Acknowledgements

This work was funded by the European Research Council under grant no. ERC-2019-CoG-864660, Critical.

## Data availability

Data will be made available on request.

## References

- [1] J.A. Boure, A.E. Bergles, L.S. Tong, Review of two-phase flow instability, *Nucl. Eng. Des.* 25 (2) (1973) 165–192.
- [2] S. Kakaç, B. Bon, A review of two-phase flow dynamic instabilities in tube boiling systems, *Int. J. Heat Mass Transfer* 51 (3–4) (2008) 399–433.
- [3] D.T. Banuti, Crossing the widom-line–supercritical pseudo-boiling, *J. Supercrit. Fluids* 98 (2015) 12–16.
- [4] Z. Wang, X. Liu, J. Chen, J. Ye, J. He, L. Jia, Y. Chen, X. Luo, An overview of flow instability at supercritical pressure, *Int. J. Heat Mass Transfer* 227 (2024) 125533.
- [5] S.K. Rai, P. Kumar, M. Tiwari, V. Panwar, D. Kumar, V.K. Sharma, A comprehensive overview of advancements, applications, and impact of supercritical fluid natural circulation loops, *Ann. Nucl. Energy* 211 (2025) 110971.
- [6] V. Garg, G. Dutta, Understanding of thermal-hydraulic instabilities and the mutual interactions at supercritical pressure, *Int. J. Heat Mass Transfer* 152 (2020) 119491.
- [7] L. Chen, X. Zhang, B. Jiang, Effects of heater orientations on the natural circulation and heat transfer in a supercritical CO<sub>2</sub> rectangular loop, *J. Heat Transf.* 136 (5) (2014) 052501.
- [8] T. Wahidi, R.A. Chandavar, A.K. Yadav, Supercritical CO<sub>2</sub> flow instability in natural circulation loop: CFD analysis, *Ann. Nucl. Energy* 160 (2021) 108374.
- [9] V. Chatoorgoon, Stability of supercritical fluid flow in a single-channel natural-convection loop, *Int. J. Heat Mass Transfer* 44 (10) (2001) 1963–1972.
- [10] P.K. Jain, Rizwan-uddin, Numerical analysis of supercritical flow instabilities in a natural circulation loop, *Nucl. Eng. Des.* 238 (8) (2008) 1947–1957.
- [11] M. Sharma, D.S. Pilkhwal, P.K. Vijayan, D. Saha, R.K. Sinha, Steady state and linear stability analysis of a supercritical water natural circulation loop, *Nucl. Eng. Des.* 240 (3) (2010) 588–597.
- [12] M. Sharma, P.K. Vijayan, D.S. Pilkhwal, D. Saha, R.K. Sinha, Linear and Nonlinear Stability Analysis of a Supercritical Natural Circulation Loop, *J. Eng. Gas Turbines Power* 132 (10) (2010) 102904.
- [13] S.K. Debrah, W. Ambrosini, Y. Chen, Discussion on the stability of natural circulation loops with supercritical pressure fluids, *Ann. Nucl. Energy* 54 (2013) 47–57.
- [14] S.K. Rai, P. Kumar, V. Panwar, Mathematical and numerical investigation of ledinegg flow excursion and dynamic instability of natural circulation loop at supercritical condition, *Ann. Nucl. Energy* 155 (2021) 108129.
- [15] W. Ambrosini, M. Sharabi, Dimensionless parameters in stability analysis of heated channels with fluids at supercritical pressures, *Nucl. Eng. Des.* 238 (8) (2008) 1917–1929.
- [16] P. Welander, On the oscillatory instability of a differentially heated fluid loop, *J. Fluid Mech.* 29 (1) (1967) 17–30.
- [17] X. Zhang, L. Chen, H. Yamaguchi, Natural convective flow and heat transfer of supercritical CO<sub>2</sub> in a rectangular circulation loop, *Int. J. Heat Mass Transfer* 53 (19–20) (2010) 4112–4122.
- [18] M. Sharma, P.K. Vijayan, D.S. Pilkhwal, Y. Asako, Steady state and stability characteristics of natural circulation loops operating with carbon dioxide at supercritical pressures for open and closed loop boundary conditions, *Nucl. Eng. Des.* 265 (2013) 737–754.

- [19] M.E. Rahman, S. Singh, Flow excursions and pressure drop oscillations in boiling two-phase channel, *Int. J. Heat Mass Transfer* 138 (2019) 647–658.
- [20] J. Yu, S. Che, R. Li, B. Qi, Analysis of ledinegg flow instability in natural circulation at supercritical pressure, *Prog. Nucl. Energy* 53 (6) (2011) 775–779.
- [21] B.T. Swapnalee, P.K. Vijayan, M. Sharma, D.S. Pikhwal, Steady state flow and static instability of supercritical natural circulation loops, *Nucl. Eng. Des.* 245 (2012) 99–112.
- [22] J. Huang, Y. Zhou, Y. Huang, Q. Luo, Y. Yuan, C. Yang, W. Hu, Experimental study of pressure drop oscillation in a supercritical carbon dioxide natural circulation loop, *Int. J. Heat Mass Transfer* 220 (2024) 125005.
- [23] P. Vijayan, M. Sharma, D. Saha, Steady state and stability characteristics of single-phase natural circulation in a rectangular loop with different heater and cooler orientations, *Exp. Therm. Fluid Sci.* 31 (8) (2007) 925–945.
- [24] D.N. Elton, U.C. Arunachala, P.K. Vijayan, Investigations on the dependence of the stability threshold on different operating procedures in a single-phase rectangular natural circulation loop, *Int. J. Heat Mass Transfer* 161 (2020) 120264.
- [25] C. T'Joene, M. Rohde, Experimental study of the coupled thermo-hydraulic-neutronic stability of a natural circulation HPLWR, *Nucl. Eng. Des.* 242 (2012) 221–232.
- [26] Y. Li, B. Yuan, W. Du, Experimental investigation of near-critical CO<sub>2</sub> heat transfer performance in a closed natural circulation loop, *Int. J. Heat Mass Transfer* 196 (2022) 123225.
- [27] G. Liu, Y. Huang, J. Wang, F. Lv, S. Liu, Experimental research and theoretical analysis of flow instability in supercritical carbon dioxide natural circulation loop, *Appl. Energy* 205 (2017) 813–821.
- [28] M. Draskic, B. Bugeat, R. Pecnik, The steady behavior of the supercritical carbon dioxide natural circulation loop, *Energy* 294 (2024) 130735.
- [29] X. Fang, Y. Xu, X. Su, R. Shi, Pressure drop and friction factor correlations of supercritical flow, *Nucl. Eng. Des.* 242 (2012) 323–330.
- [30] M.M. Ehsan, Z. Guan, A.Y. Klimenko, A comprehensive review on heat transfer and pressure drop characteristics and correlations with supercritical CO<sub>2</sub> under heating and cooling applications, *Renew. Sustain. Energy Rev.* 92 (2018) 658–675.
- [31] X. Fang, L. Xu, Y. Chen, W. Chen, Correlations for friction factor of turbulent pipe flow under supercritical pressure: Review and a new correlation, *Prog. Nucl. Energy* 118 (2020) 103085.
- [32] S.S. Pitla, D.M. Robinson, E.A. Groll, S. Ramadhyani, Heat transfer from supercritical carbon dioxide in tube flow: a critical review, *Hvac R Res.* 4 (3) (1998) 281–301.
- [33] J.Y. Yoo, The turbulent flows of supercritical fluids with heat transfer, *Annu. Rev. Fluid Mech.* 45 (1) (2013) 495–525.
- [34] S. Zhang, X. Xu, C. Liu, C. Dang, A review on application and heat transfer enhancement of supercritical CO<sub>2</sub> in low-grade heat conversion, *Appl. Energy* 269 (2020) 114962.
- [35] Q. Wang, J. Xu, C. Zhang, B. Hao, L. Cheng, A critical review on heat transfer of supercritical fluids, *Heat Transf. Eng.* 44 (21–22) (2023) 1969–1994.
- [36] N.E. Petrov, V.N. Popov, Heat-transfer and resistance of carbon-dioxide being cooled in the supercritical region, *Therm. Eng.* 32 (3) (1985) 131–134.
- [37] P. Jiang, Y. Zhang, Y. Xu, R. Shi, Experimental and numerical investigation of convection heat transfer of CO<sub>2</sub> at supercritical pressures in a vertical tube at low Reynolds numbers, *Int. J. Therm. Sci.* 47 (8) (2008) 998–1011.
- [38] H. Nemati, A. Patel, B.J. Boersma, R. Pecnik, Mean statistics of a heated turbulent pipe flow at supercritical pressure, *Int. J. Heat Mass Transfer* 83 (2015) 741–752.